Check for updates

Elevated electrochemical performances enabled by a core–shell titanium hydride coated separator in lithium–sulphur batteries†

Zhiyuan Zhao, Xiaobo Duan, [ID] * Lei Zhang, Zhiwei Che, Kun Wang, Bin Zheng [ID] * and Xiaogang Wang

To date, the lithium–sulphur battery is still suffering from fast capacity fade and poor rate performance due to its special electrochemical mechanism. The interlayer or separator with conductive coatings is considered effective in inhibiting the shuttle effect. Here, we proposed a novel metal hydride with high conductivity and preferably chose TiH_2 as the conductive coating because of its low cost, high conductivity, and good stability in air. The TiH_2 powder was prepared by a simple ball-milling method, and the effect of the atmosphere was also investigated. A core–shell heterostructure formed, in which the TiH_2 core acted as an electron transfer pathway, and the titanium oxide nano-shell functioned as the absorber for polysulfides. Thus, with the combination of fast electronic transfer and strong absorption ability, the TiH_2 coated separator could improve the cycling stability, the rate performances, and the self-discharge rate. The TiH_2 separator could increase the capacity of the lower plateau and delay the oversaturation points at high rates, promoting the liquid–solid conversion. It is believed that the promotion resulted from the high conductivity and polysulfide absorption of the TiH_2 separator. Although the preparation process still needs further optimization, the core–shell metal hydride provided a novel strategy for designing the heterostructure, which could provide high conductivity and strong absorption ability toward polysulfides simultaneously.

Introduction

The lithium–sulphur battery is considered one of the most promising high-energy batteries due to its high theoretical energy density (2600 W h kg^{-1}), low cost, and environmental sustainability. However, the sluggish kinetics and the poor cycle stability resulting from the insulating nature of solid sulphur species and the unlimited diffusion of polysulfides are hindering the commercialisation of the lithium–sulphur battery. Polysulfide intermediates, the most important difference between lithium–sulphur batteries and other battery systems, are believed to play a positive role in promoting the sulphur conversion reaction as the redox mediators, but also corrode the metallic lithium and cause the irreversible loss of sulphur species, giving researchers a dilemma.[1] So, how to manage polysulfides rationally is a key issue in the lithium–sulphur battery.

In the last years, great progress has been made to solve these problems. The detailed methods include (1) using porous materials as hosts;[2–6] (2) designing new electrolytes;[7–9] (3) protecting the metallic lithium anode from the corrosion of polysulfides;[10–13] (4) polysulfide-inhibiting interlayer or separator.[14–16] Among them, the specially designed separator or interlayer usually traps polysulfides by physical and chemical confinement and also reactive the dead sulphur species, boosting the electrochemical performances of lithium–sulphur batteries. A typical polysulfide-inhibiting interlayer or functioned separator is covered by conductive materials, commonly carbonaceous materials, due to its low cost and adequate conductivity. For example, Arumugam Manthiram proposed the MWCNT interlayer in lithium–sulphur batteries firstly, reduced the charge transfer resistance of the sulphur cathodes and the loss of the dissolved intermediates.[17] Yi Cui compared the effects of conductive materials as polysulfides barrier on the electrochemical performances and discovered that higher electronic conductivity of the coated separators resulted in greater improvements.[18]

Despite the progress obtained, the weak interaction of nonpolar carbon with polysulfides results in a poor trap of polysulfides, causing the corrosion of lithium anode and the loss of active materials. Many researchers turn their attention to polar compounds gradually, such as oxides,[19,20] sulfides,[21,22] metal–boron compounds,[23,24] metal–C compounds,[25,26] which exhibit the stronger absorption and catalytic ability for

Department of Materials Science & Engineering, Xi'an University of Science and Technology, Xi'an 710054, China. E-mail: xiaobo12558@163.com; zhengbin@xust.edu.cn

polysulfides. TiO$_2$, a typical polar semi-conducting oxide, has been studied intensively in lithium–sulphur batteries. Its absorption ability and electrical conductivity could be enhanced by band engineering including doping and oxygen defects.[27] However, TiO$_2$ has no adequate conductivity even after modification and must couple with conductive carbon materials. Thus, these materials exhibiting strong interactions with polysulfides and high conductivities are preferred. Consequently, other titanium compounds, such as TiC,[28] TiB$_2$,[23] TiN,[29,30] Ti$_4$O$_7$,[31] TiO,[32] Ti$_2$O,[33] have attracted great attention.

Herein, we proposed a novel material system, transition metal hydrides, as the conductive coating on the Celgard separators. These hydrides usually exhibit excellent electron conductivities and were easily ground to fine powder due to their high fragility. TiH$_2$, one of the cheapest and most stable metal hydrides in the ambient atmosphere, was preferentially chosen as the conductive coating on the separator here because it exhibits an excellent conductivity ($\sim$10^4 S cm^{-1})[34] and can be sufficiently supplied at a large scale in the titanium metallurgy industry. Moreover, it also exhibits high fragility, which means that the fine TiH$_2$ powder can be produced mechanically at a low cost. During the preparation process, a titanium oxide nano-film *in situ* formed in air and covered the TiH$_2$ core due to the medium activity of titanium hydride toward oxygen. The core–shell microstructure combined the high electron conductivity of TiH$_2$ with the absorption ability of polar titanium oxides. Unsurprisingly, the TiH$_2$ coated separator could improve the electrochemical performance of the lithium–sulphur battery.

Experimental

Preparation of the TiH$_2$ coated separators

The purchased commercial TiH$_2$ raw powder ($\sim$100 mesh) was milled for 2 hours in an Ar-filled MSK-SFM-3 high energy ball miller with a ball material ratio of 5 : 1. 0.9 g milled powder was mixed with 0.1 g PVDF (polyvinylidene fluoride), and then an appropriate amount of NMP (1-methyl-2-pyrrolidinone) was added to form a viscous slurry. The slurry was coated on the commercial separators (Celgard 2520) with the doctor blade coater. The coated separator was heated for 12 hours under vacuum to remove NMP and then cut into the disks with diameters of 18 mm. The TiH$_2$ loading was controlled to $\sim$1.5 mg cm^{-2}.

Preparation of the sulphur cathodes

Typically, 0.7 g commercial sulphur powder was mixed with 0.2 g carbon black (EC-300J) and heated at 150 °C for 10 hours. The obtain S/C powder was ground and mixed with 0.1 g PVDF. Then, an appropriate amount of NMP was also added to form a viscous slurry. The slurry was coated on Al foil with a doctor blade coater. The sulphur cathode was dried at 60 °C for 24 h in air and cut into disks after drying. The sulphur loading was controlled to 2.7–3 mg cm^{-2}.

Electrochemical measurement

The CR2025 coin cell was assembled in argon filled glove box with moisture and oxygen contents of <0.1 ppm. A lithium metal foil was used as the counter electrode and a solution of 1 M bis(trifluoromethane)sulfonamide lithium salt (LiTFSI) and 2 wt% LiNO$_3$ dissolved in dimethoxymethane (DME): 1,3-dioxolane (DOL) (v/v = 1 : 1) mixture.

The charge–discharge measurements were performed at Land 2001A battery tester at various rates, where 1C was set to 1675 mA g^{-1}. The electrochemical impedance measurements were carried out using a CHI 660D electrochemical workstation at open-circuit voltage with a voltage of amplitude of 10 mV and a frequency range from 0.1 to 10^5 Hz. The cyclic voltammetry measurements were also conducted at CHI 660D electrochemical workstation with a voltage window of 1.7–3.0 V at various scan rates.

Polysulfide adsorption study and XPS sample preparation

0.02 M Li$_2$S$_6$ solution was prepared by adding an appropriate amount of Li$_2$S and S$_8$ in DME solution with stirring at room temperature. 0.5 g TiH$_2$ powder was added in 4.2 mL Li$_2$S$_6$ solution to inspect the colour change after 10 min standing. Afterwards, the solution was filtered and the solids for XPS analysis were obtained after drying *in vacuo* for 10 h.

Material characterization

The morphology and structure were investigated by field emission scanning electron microscopy (FE-SEM, Zeiss) and field-emission transmission electron microscopy (TEM, JEM-2800) coupled with Energy Dispersive Spectrometer (EDS). The electrical conductivities were measured by a standard four-point-probe powder resistivity measurement system (ST2253) with a pressure of 10 Mpa. The phases of TiH$_2$ powder were determined by X-ray diffraction (XRD, Shimadzu 7000). X-ray photoelectron spectroscopy (XPS) measurements were performed on Kratos Thermo Scientific K-Alpha+ instrument coupled with an Ar-filled glovebox for the sample transfer under Ar protection, using monochromated Al Kα X-rays as the excitation source with an accelerating voltage of 15 kV and a beam of 15 mA. The ionic conductivity measurements of the separators were carried out on CHI660D *via* the impedance–time method (1 kHz) according to the reported calculation equation.[35,36] The polysulfides diffusion test was carried out in an H type cell. The left chamber was filled with 0.02 mol L^{-1} Li$_2$S$_6$ DME solution and the right was pure DME solution. The separator was placed between the left and the right chamber.

Results and discussion

Commercial TiH$_2$ powder is usually supplied as raw and coarse particles, which is considered detrimental to the absorption of polysulfides due to its low specific surface area. Reducing the sizes of the commercial TiH$_2$ particles is vital. Fortunately, TiH$_2$ exhibits extremely high fragility, which favours reducing the particle sizes mechanically by a simple ball milling method. Fig. 1 shows the XRD patterns of the purchased TiH$_2$ powder milled in Ar and air. The anatase TiO$_2$ peaks are obvious in the XRD pattern of TiH$_2$ milled in air, indicating that TiH$_2$ powder was easily oxidized after ball milling in air due to its high
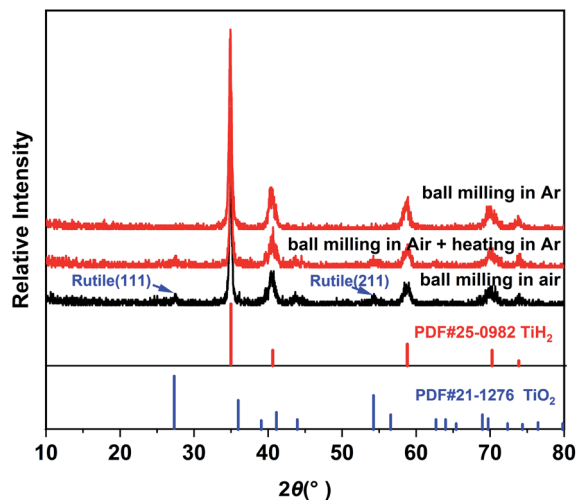
Fig. 1 XRD patterns of TiH$_2$ powders ball milled and heated in air or Ar.

activity toward oxygen. Undoubtedly, too much TiO$_2$ on the surface of the TiH$_2$ particles would lower the electron transfer kinetics. After being milled in air, the TiH$_2$ powder showed a dramatically decreased conductivity of 0.000458 S cm^{-1} (Fig. 2), suggesting the negative role of the TiO$_2$. The microstructure of the TiH$_2$ milled in air and Ar was similar (Fig. S1†), implying the dramatic decrease of the conductivity should be associated with the formation of TiO$_2$ rather than the microstructure change. Even after heated in Ar, the oxidized TiH$_2$ powder was not resumed completely. The anatase TiO$_2$ peaks were still obvious and the increased conductivity of 0.0192 S cm^{-1} was still insufficient for lithium–sulphur batteries. Accordingly, the inert atmosphere was considered essential to obtain highly conductive TiH$_2$ powder in the ball milling process. Under the protection of the Ar atmosphere, no obvious characteristic peak of Ti–O compounds was observed. Correspondingly, the milled TiH$_2$ powder exhibited rather high conductivity (23 S cm^{-1}), approaching the level of the raw TiH$_2$ powder and even higher than carbon black and Ti$_4$O$_7$.[37,38] The conductivity was considered rather suitable for the coated
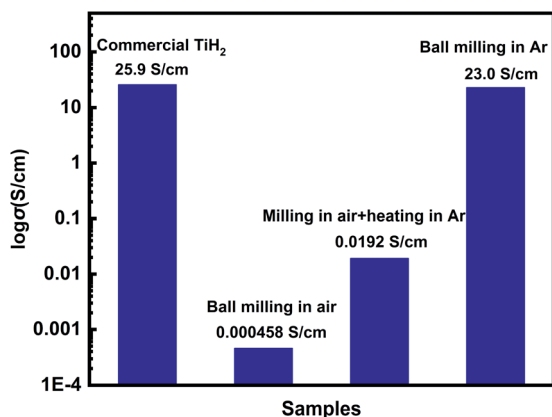
separator in lithium–sulphur batteries. Similarly, the conductivities of the commercial Ti$_4$O$_7$ powder milled in Ar or air were also measured and the results highlighted the importance of inert atmosphere during milling (Fig. S2†).

The XPS spectra of TiH$_2$ powder milled in Ar could provide more information about the chemical composition and states on the surface of the TiH$_2$ powder. According to the chemical composition information shown in Table S1,† the oxygen content was rather higher unexpectedly. The Ti 2p spectra (Fig. 3a) also show typical Ti 2p$_{1/2}$ and Ti 2p$_{3/2}$ peaks for Ti^{4+} ions, just like the spectrum of nano TiO$_2$, indicating that a titanium oxide layer formed on the surface of the TiH$_2$ particles. Besides the Ti^{4+} peaks, the typical Ti^0 peak also was observed, implying that the thickness of the titanium oxide layer was at the nanometer scale because the detective depth of XPS is only several nanometers. The O 1s spectra (Fig. 3b) show that the titanium oxide layer formed at room temperature contained more oxygen defects than the commercial nano TiO$_2$ particles, indicating that the crystallization degree was lower. According to the previous work,[27] the oxygen defects could narrow the bandgap of TiO$_2$, trap polysulfides, and accelerate the polysulfides conversion. Thus, the oxygen defect-rich TiO$_{2-x}$ could be considered beneficial for the cycle and rate performances in lithium–sulphur batteries.[39–43]

Considering the important role of the surface in absorption and catalytic behaviours, SEM and TEM were used to explore the titanium oxide layer, as shown in Fig. 4. Fig. 4a shows that the TiH$_2$ particle sizes ranged from several micrometres to sub-micrometres. In the higher magnitude view provided by TEM (Fig. S3†), the existence of the formed oxide layer was evidenced by the Ti and O mapping. Further, the HRTEM image (Fig. 4b) shows the oxide layer had a low crystallinity degree, distinguished from the ordered TiH$_2$ core. The corresponding SAED pattern in Fig. 4c only reveals the clear diffraction spots indexed as (111) plane of TiH$_2$ ($Fd\bar{3}m$). The oxide layer revealed no obvious electron diffraction spots, which may result from its lower amount and disordered characteristic. Because the oxide layer covered on the TiH$_2$ particles was as thin as ~5 nm, the electron could still transfer through the oxide layer by the quantum tunnelling effects, thus the TiH$_2$ powder remained highly conductive. The surface of the commercial TiH$_2$ powder was examined by XPS, SEM and TEM, which were shown in Fig. S4.† The results also showed the existence of the nano Ti–O layer on the commercial TiH$_2$ particles, indicating the nano Ti–
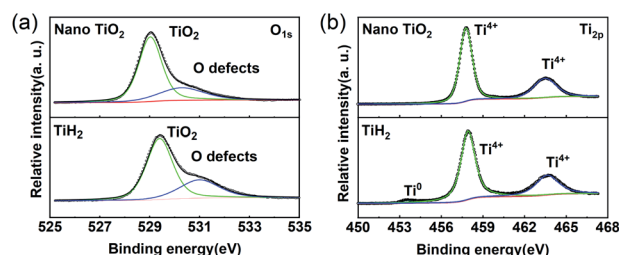

Fig. 2 The electron conductivities of the TiH$_2$ powder treated by various processes.

Fig. 3 XPS spectra of the nano TiO$_2$ and TiH$_2$ powder. (a) Ti 2p. (b) O 1s.
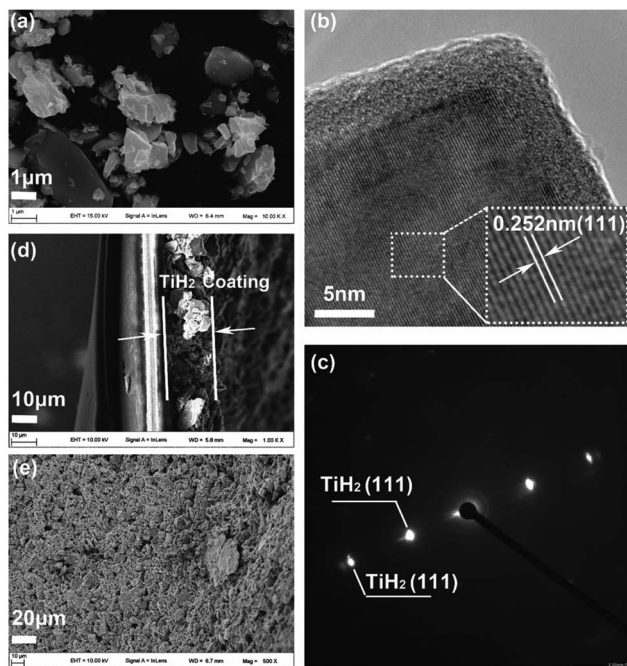
Fig. 4 Microstructure analysis of the TiH$_2$ powder (a–c) and TiH$_2$ coated separator (d and e).

Fig. 5 XPS spectra of the TiH$_2$ powder soaked in Li$_2$S$_6$ solution. (a) C 1s. (b) Ti 2p (c) O 1s. (d) S 2p.

O layer formed spontaneously when the TiH$_2$ particles were exposed to air, even at room temperature. The Ar atmosphere during milling could limit the formation of titanium oxides, avoiding the dramatic decrease of the electrical conductivity. However, air could cause too severe oxidation, even to the extent that the titanium oxides could be detected by XRD. Unsurprisingly, the electrical conductivity of the TiH$_2$ powder milled in air decreased dramatically. Fig. 4d and e show the cross-section and surface images of the TiH$_2$ separator. It can be seen that a porous TiH$_2$ layer of 15–20 μm covered the commercial plastic separator.

Since a disordered TiO$_2$ nanofilm covered the TiH$_2$ core, the previous researches on the polysulfides absorption characteristics of TiO$_2$ could provide more guides. It is well known that TiO$_2$ with oxygen defects is a good polysulfide absorber. Unsurprisingly, the TiH$_2$ powder also exhibited its absorption ability of polysulfide in Li$_2$S$_6$ solution due to its Ti–O shell (Fig. S5†). Here, XPS also were used to clarify the absorption mechanism of the polysulfides. ∼0.55 eV chemical shift is observed in the Ti 2p spectrum after the TiH$_2$ powder absorbed polysulfides (Fig. S6†). The blue chemical shift was also observed in other titanium oxides due to the electron transfer from Li$_2$S$_n$ to Ti–O.[43] This blue shift was used to verify the presence of Ti–S interaction by some researchers.[27] Meanwhile, the intensive S–O peaks in S 2p and O 1s spectra were discovered (Fig. 5c and d), which meant the polysulfides were absorbed on the titanium oxide layer via S–O interaction mainly. In previous researches, all the S–O interaction, Li–O interaction, and Ti–S interaction were discovered in the absorption of polysulfides on titanium oxides, but the dominating interaction is still controversial. For example, some researchers[44] assumed
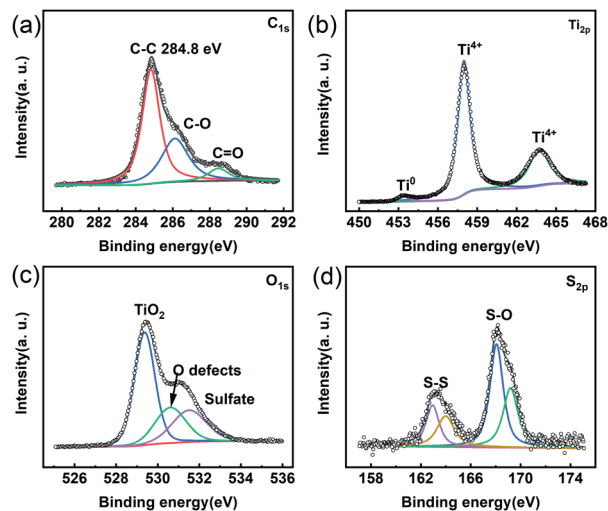
TiO$_2$ bound polysulfides via metal–S interaction instead of the S–O interaction because its redox potential fell out the redox potential window of polysulfides. Shujiang Ding et al. concluded that the Li–O and Ti–S interaction played an important role in binding the polysulfides on the surface of the CNT@TiO$_{2-x}$ composite.[27] Xin Wang et al. revealed that the S–O peaks occurred before cycling while the Ti–S peak also appeared after cycling, but the detailed mechanism was not fully elucidated.[41,45] However, Ning Liu et al. discovered the opposite results.[46] Despite the uncertain mechanism, intensive researches have proved TiO$_2$ to be a strong absorber toward polysulfides. Here, the TiO$_{2-x}$ nano-shell also proved its similar role. Thus, The TiH$_2$ powder coated separator also exhibited a better polysulfides-inhibiting property compared with the Celgard separator, as shown in Fig. S7.†

As a coating material in the lithium–sulphur battery, the electrochemical stability was firstly evaluated, as shown in Fig. S8.† It can be seen that the TiH$_2$ powder itself delivered a low specific capacity (∼5 mA h g^{-1}) in 1–3 V, mainly from its capacitive charge/discharge behaviour. The TiH$_2$ powder showed admirable electrochemical stability.

Besides electrochemical stability, ionic conductivity is also an important issue for separators. The TiH$_2$ and Celgard separator was 0.74 mS cm^{-1} and 0.64 mS cm^{-1}, whereas the total ionic resistance was 3.65 Ω and 1.98 Ω (Table S2†). The total ionic resistance may be a better quantitative parameter for these separators due to their different thickness. Because of the higher thickness, the TiH$_2$ separator exhibited higher total ionic resistance.

As the previous works reported, highly conductive materials coated separators were usually beneficial to the cycling performances of the lithium–sulphur battery, but whether the higher ionic resistance would deteriorate the electrochemical performances needed to be explored. Fig. 6 shows the electrochemical performances of the lithium–sulphur batteries with Celgard and TiH$_2$ separators during cycling. For simplicity, the lithium–
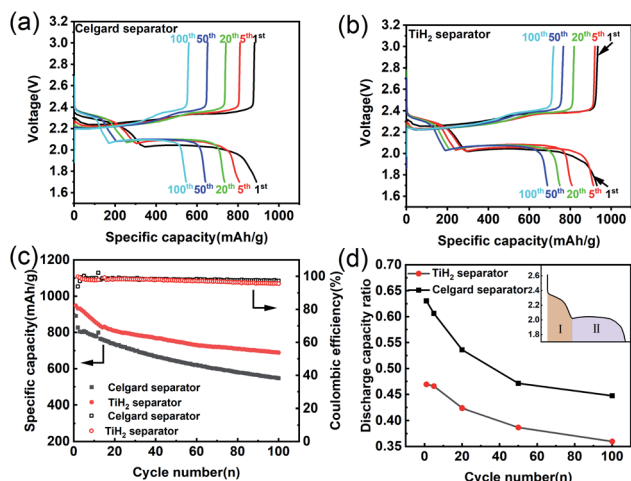
Fig. 6 Electrochemical performances of lithium–sulphur batteries with Celgard and TiH$_2$ separators during cycling. (a and b) Discharge/charge profiles of the lithium–sulphur batteries with the Celgard and TiH$_2$ separators. (c) Cycling stability of the lithium–sulphur batteries at 0.2C. (d) Ratio changes of the specific discharge capacity contributed by the upper and the lower plateau (Q_{upper}/Q_{lower}) during cycling.

sulphur batteries with Celgard and TiH$_2$ separators were named the Celgard battery and the TiH$_2$ battery, respectively. From Fig. 6a and b, it can be seen that the lithium–sulphur batteries exhibited similar initial capacities. However, the lithium–sulphur battery with Celgard separator degraded rapidly during cycling, especially in the initial stage. By contrast, the capacity of the lithium–sulphur battery with TiH$_2$ separator degraded more slowly (Fig. 6c) and the increase of the discharge/charge polarizations were not observed during cycling, so the degradation cannot be attributed to the changes of the electrode's polarization. To explore the detailed degradation mechanism of the sulphur cathodes, we divided the discharge profiles into two regions according to the upper and lower voltage plateaus, corresponding to the $S_8 \rightarrow Li_2S_4$ and the $Li_2S_4 \rightarrow Li_2S$ conversion process respectively, as shown in Fig. 6d. For simplicity, the capacities contributed by the upper and lower voltage plateaus were named Q_{upper} and Q_{lower}. From Fig. 6d, it can be seen that the ratios (Q_{upper}/Q_{lower}) for the two batteries both decreased during cycling, indicating that the lower voltage plateau degraded more rapidly compared with the upper voltage plateau. However, the initial Q_{upper}/Q_{lower} ratio for the Celgard battery was higher and decreased more rapidly, consistent with the results shown in Fig. 6a and b. It can be seen that the upper voltage plateau contributed more capacity in the TiH$_2$ battery. It meant that the soluble long-chain polysulfides would react with the lithium anode for a longer time, promoting the S-containing species loss. Thus, the capacity decay rate of the Celgard battery increased inevitably. These phenomena could be explained by the inhibition behaviour of polysulfides from the TiH$_2$ separator.

It is well known that the side-reaction of the long-chain polysulfides with metallic lithium should be responsible for severe self-discharge in lithium–sulphur batteries as well as the fast fading during cycling. Whether the polysulfides-inhibiting

of the TiH$_2$ separator would also improve the self-discharge performance was worth investigating. Fig. S9† shows their self-discharge performances. In the TiH$_2$ battery, its open-circuit voltage decreased more slowly and the capacity loss was also smaller than the Celgard batteries after 200 h standing. This improvement could also prove the positive role of the TiH$_2$ separator in suppressing the dissolution of polysulfides.

Besides the better cycle stability and self-discharge rate, it was also expected that the TiH$_2$ separator could offer better rate performance due to its high electron conductivity from the TiH$_2$ core and the absorption ability from the TiO$_{2-x}$ shell. The electrochemical performances of the lithium–sulphur batteries at various rates were shown in Fig. 7. In Fig. 7a and b, the TiH$_2$ separator showed its advantages in capacities and polarizations at various rates, especially at 0.5C or higher rates. By comparison, at 0.5C or higher rates, the Celgard battery suffered from severe capacity degradation, which mainly resulted from the fading on the lower voltage plateau (Fig. 7a and b). At 1C and higher rates, the lower voltage plateau even disappeared.

In the discharge process, the upper plateau is usually assigned to the electrochemical conversion reaction from S_8 to Li_2S_4, which has better reaction kinetics compared with the Li_2S_4 to Li_2S conversion that occurred in the lower plateau. So, the lower plateau is more sensitive to the discharge rates and
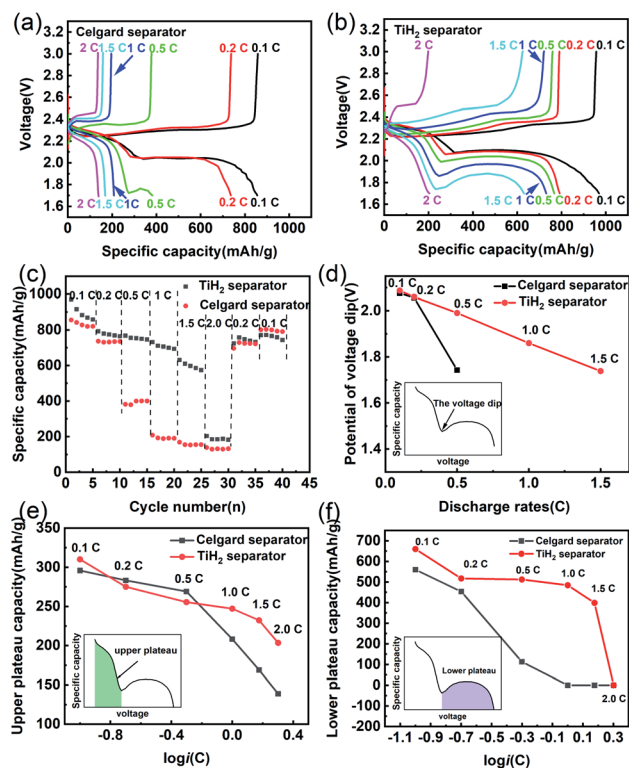

Fig. 7 Electrochemical performances of the lithium–sulphur batteries at various discharge/charge rates. Discharge/charge profiles of the Celgard battery (a) and the TiH$_2$ battery (b). (c) Specific capacity of the lithium–sulphur batteries at various discharge/charge rates. (d) Relationship between the initial Li$_2$S deposition potentials and the discharge rates. Relationship between Q_{upper} (e), Q_{lower} (f), and the discharge rates (i).

degraded faster at high rates. If the initial potential of the lower plateau, also called the voltage dip or the oversaturation point by some researchers,[47,48] dropped below 1.7 V, the lower plateau would disappear, leading to the sharply dropped capacity, as shown in Fig. 7c. The oversaturation point corresponds to the barrier for the initial nucleation of Li_2S and can be diminished by some redox mediators which promote the formation of Li_2S.[49] Fig. 7d shows the relationship between the oversaturation points and the discharge rates, and an approximately linear relationship can be observed in the TiH_2 battery. At 0.1C and 0.2C, the oversaturation points occurred at similar potentials in the two batteries. When the discharge current increased to 0.5C, the oversaturation points in the Celgard battery dropped sharply and out of the cut-off voltage window at higher rates. It seems that the TiH_2 separator could promote the nucleation of the solid discharge phase and thus diminish the voltage dip at the oversaturation points.

Fig. 7e and f show the capacities contributed by the upper and lower voltage plateau at various discharge rates, respectively. The approximative logarithmic relationship between the capacities contributed by the upper plateau (Q_{upper}) and the discharge rates (i) was discovered in Fig. 7e, which indicated that the polarization probably resulted in the capacity decrease of the upper voltage plateau. In the Celgard battery, a sudden capacity fall was observed when the current increased to 0.5C. At higher rates, the capacities fell to zero due to the huge voltage dip. By contrast, the capacities contributed by the lower plateau remained relatively stable until the rate increased to 2C.

Based on the above description, it seems the lower plateau rather than the upper plateau had the primary responsibility for the huge rate differences between the Celgard battery and the TiH_2 battery. Unlike the upper plateau, no apparent linear relationship between the capacities (Q_{lower}) and log i could be observed, indicating the capacity contributed by the lower plateau (Q_{lower}) was affected by other factors, besides the polarization associated with the discharge rates. Yan Zhao[42] studied the effect of the oxygen defects in TiO_{2-x} on the polysulfides immobilization and catalytic conversion reactions by the first-principles computational characterization and experimental design. It was revealed that TiO_2, especially the TiO_{2-x} with oxygen defects, was capable of absorbing and catalysing the S-containing species, thus accelerating the transformation of S_8 to Li_2S. Other researchers obtained a similar conclusion on TiO_{2-x}. Regardless of the detailed mechanism, it is quite certain that TiO_{2-x} can absorb and catalyse the S-containing species. However, it was usually coupled with high conductive carbonaceous materials due to its poor conductivity. Some other metal oxides, such as VO_2,[50] MnO_2,[51] could also promote the polysulfides conversion via the S–O interaction. So, it could be inferred that the core–shell $TiO_{2-x}@TiH_2$ structure could combine the absorption and catalytic properties from the TiO_{2-x} shell and the high conductivity from the TiH_2 core, improving the electrochemical performances.

The CV tests with different scan rates were performed to study the reaction kinetic behaviours of the lithium–sulphur batteries with different separators. Consistent with the rate performances showed in Fig. 7, the lithium–sulphur battery with the TiH_2 separator shows smaller polarizations and higher peak currents at various scan rates except for peak I, which was assigned to the conversion from S_8 to Li_2S_4 (Fig. S10†). First, compared with the fast conversion from S_8 to Li_2S_4, the conversion of Li_2S_4 to Li_2S is more easily affected by the various eternal factors due to its sluggish kinetics. Second, it is also accepted that the charging process is relatively slower than the discharge process.[37] So, it is easily understood why the TiH_2 separator influenced the peaks differently. To further evaluate the effect of the TiH_2 separator on the reaction kinetics quantitatively, the CV data were characterized by analysing the plots of i_p vs. $v^{0.5}$ according to the Randles–Sevcik equation at 298 K:[52]

$$i_p = 268600 n^{\frac{3}{2}} A D^{\frac{1}{2}} C v^{\frac{1}{2}}$$

where i_p is the measured peak currents; v is the scan rates used; n is the transfer number of electrons involved in the reaction; A is the electrode surface area; C is the bulk concentration of the reactant. The lithium–sulphur battery undergoes the complex electrochemical and chemical disproportionation conversion, involving the diffusion of the polysulfides and lithium ions simultaneously in the electrolyte and the electrodes, so the CV data can reflect the lithiation/delithiation kinetics. In Fig. 8c and d, the TiH_2 separator brought about a slightly lower slope for peak I ($|a_I|$) and a higher slope for the peak II, agreeing with its discharge profiles shown in Fig. 6b and 7b. The higher slope of the fitting line ($|a_{III}|$ and $|a_{IV}|$) also indicated the positive role of the TiH_2 separator in promoting the corresponding reactions during charging. The EIS results also proved the positive effect on the kinetics of the sulphur cathodes brought by the TiH_2 separator (Fig. S11†). It also can be concluded that the higher ionic resistance of the TiH_2 separator would not deteriorate the electrochemical performances due to the benefits brought by the absorption property and high conductivity of the TiH_2 powder.
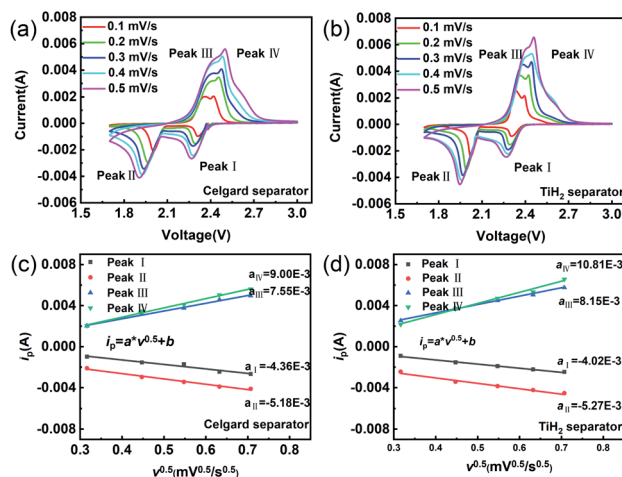

Fig. 8 Cyclic voltammetry of the lithium−sulphur batteries with Celgard separator (a) and TiH_2 separator (b). Relationship between the oxidation/reduction peak currents and the scan rates in the lithium−sulphur batteries with Celgard separators (c) and TiH_2 separators (d).

Conclusions

A highly conductive titanium hydrogen powder with the core–shell microstructure was prepared by a facile, simple ball-milled method in Ar. The *in situ* formation of the core–shell structure could be attributed to the slight oxidation of the TiH_2 powder and allowed the fast electronic transfer due to the quantum effect. As a polar titanium oxide layer, the shell also exhibited a strong absorption ability to the polysulfides, just like the titanium oxides in other works. The TiH_2 coated separator could enhance the comprehensive electrochemical performance remarkably, including the cycling stability, rate performances, and self-discharge rates. It was concluded that these improvements resulted from the absorption of the polysulfide on the titanium oxide nano-shell, which could absorb the polysulfides and promote the conversion from soluble polysulfides to Li_2S_2 or Li_2S. After further optimization, better polysulfide absorption and electronic transfer properties can be expected. Meanwhile, based on a similar principle, other transition metal hydrides can be used to form a corresponding core–shell microstructure. The shell should not be limited in the scope of oxides. Other compounds exhibiting strong affinities toward polysulfides are also optional. By controlling the atmosphere exposed during preparation, various core–shell heterostructures might be created and play more important roles in absorbing or catalysing the sulphur conversion.

Conflicts of interest

There are no conflicts to declare.

Acknowledgements

Notes and references

1 G. Li, S. Wang, Y. Zhang, M. Li, Z. Chen and J. Lu, *Adv. Mater.*, 2018, **30**, 1705590.
2 H. Choi, X. Zhao, D. S. Kim, H. J. Ahn, K. W. Kim, K. K. Cho and J. H. Ahn, *Mater. Res. Bull.*, 2014, **58**, 199–203.
3 Z. Xiao, D. Kong, Q. Song, S. Zhou, Y. Zhang, A. Badshah, J. Liang and L. Zhi, *Nano Energy*, 2018, **46**, 365–371.
4 Z. Zheng, H. Guo, F. Pei, X. Zhang, X. Chen, X. Fang, T. Wang and N. Zheng, *Adv. Funct. Mater.*, 2016, **26**, 8952–8959.
5 L. Ji, M. Rao, S. Aloni, L. Wang, E. J. Cairns and Y. Zhang, *Energy Environ. Sci.*, 2011, **4**, 5053–5059.
6 K. Gao, X. Guo, B. Zheng, J. Wang and L. Wang, *Mater. Today Energy*, 2021, **20**, 100458.
7 L. Suo, Y. S. Hu, H. Li, M. Armand and L. Chen, *Nat. Commun.*, 2013, **4**, 1–9.
8 M. Cuisinier, P. E. Cabelguen, B. D. Adams, A. Garsuch, M. Balasubramanian and L. F. Nazar, *Energy Environ. Sci.*, 2014, **7**, 2697–2705.
9 H. Lu, Y. Zhu, Y. Yuan, L. He, B. Zheng, X. Zheng, C. Liu and H. Du, *J. Mater. Sci.: Mater. Electron.*, 2021, **32**, 5898–5906.
10 H. Kim, J. T. Lee, D. C. Lee, M. Oschatz, W. il Cho, S. Kaskel and G. Yushin, *Electrochem. Commun.*, 2013, **36**, 38–41.
11 H. K. Jing, L. L. Kong, S. Liu, G. R. Li and X. P. Gao, *J. Mater. Chem. A*, 2015, **3**, 12213–12219.
12 B. Duan, W. Wang, H. Zhao, A. Wang, M. Wang, K. Yuan, Z. Yu and Y. Yanga, *ECS Electrochem. Lett.*, 2013, **2**, A47.
13 C. Yan, X. B. Cheng, C. Z. Zhao, J. Q. Huang, S. T. Yang and Q. Zhang, *J. Power Sources*, 2016, **327**, 212–220.
14 T. G. Jeong, Y. H. Moon, H. H. Chun, H. S. Kim, B. W. Cho and Y. T. Kim, *Chem. Commun.*, 2013, **49**, 11107–11109.
15 B. Li, Z. Sun, Y. Zhao, Y. Tian, T. Tan, F. Gao and J. Li, *J. Nanopart. Res.*, 2019, **21**, 1–10.
16 S. H. Chung and A. Manthiram, *J. Phys. Chem. Lett.*, 2014, **5**, 1978–1983.
17 Y. S. Su and A. Manthiram, *Chem. Commun.*, 2012, **48**, 8817–8819.
18 H. Yao, K. Yan, W. Li, G. Zheng, D. Kong, Z. W. Seh, V. K. Narasimhan, Z. Liang and Y. Cui, *Energy Environ. Sci.*, 2014, **7**, 3381–3390.
19 Z. Xiao, Z. Yang, L. Wang, H. Nie, M. Zhong, Q. Lai, X. Xu, L. Zhang and S. Huang, *Adv. Mater.*, 2015, **27**, 2891–2898.
20 L. Luo, X. Qin, J. Wu, G. Liang, Q. Li, M. Liu, F. Kang, G. Chen and B. Li, *J. Mater. Chem. A*, 2018, **6**, 8612–8619.
21 Y. Yang, S. Wang, L. Zhang, Y. Deng, H. Xu, X. Qin and G. Chen, *Chem. Eng. J.*, 2019, **369**, 77–86.
22 S. Yao, J. Cui, J. Q. Huang, Z. Lu, Y. Deng, W. G. Chong, J. Wu, M. Ihsan Ul Haq, F. Ciucci and J. K. Kim, *Adv. Energy Mater.*, 2018, **8**, 1800710.
23 L. Jin, J. Ni, C. Shen, F. Peng, Q. Wu, D. Ye, J. Zheng, G. Li, C. Zhang, Z. Li and J. P. Zheng, *J. Power Sources*, 2020, **448**, 227336.
24 C. Li, X. Liu, L. Zhu, R. Huang, M. Zhao, L. Xu and Y. Qian, *Chem. Mater.*, 2018, **30**, 6969–6977.
25 W. Cai, G. Li, K. Zhang, G. Xiao, C. Wang, K. Ye, Z. Chen, Y. Zhu and Y. Qian, *Adv. Funct. Mater.*, 2018, **28**, 1704865.
26 C. Lin, W. Zhang, L. Wang, Z. Wang, W. Zhao, W. Duan, Z. Zhao, B. Liu and J. Jin, *J. Mater. Chem. A*, 2016, **4**, 5993–5998.
27 Y. Wang, R. Zhang, J. Chen, H. Wu, S. Lu, K. Wang, H. Li, C. J. Harris, K. Xi, R. V. Kumar and S. Ding, *Adv. Energy Mater.*, 2019, **9**, 1900953.
28 J. Zhao and Z. Yan, *J. Alloys Compd.*, 2021, **856**, 156609.
29 Z. Hao, L. Yuan, C. Chen, J. Xiang, Y. Li, Z. Huang, P. Hu and Y. Huang, *J. Mater. Chem. A*, 2016, **4**, 17711–17717.
30 W. G. Lim, C. Jo, A. Cho, J. Hwang, S. Kim, J. W. Han and J. Lee, *Adv. Mater.*, 2019, **31**, 1–9.
31 Y. Guo, J. Li, R. Pitcheri, J. Zhu, P. Wen and Y. Qiu, *Chem. Eng. J.*, 2019, **355**, 390–398.
32 Z. Li, L. Tang, X. Liu, T. Song, Q. Xu, H. Liu and Y. Wang, *Electrochim. Acta*, 2019, **310**, 1–12.
33 R. Wang, K. Wang, H. Tao, W. Zhao, M. Jiang, J. Yan and K. Jiang, *J. Mater. Chem. A*, 2020, **8**, 11224–11232.
34 S. P. Murarka, S. H. Ko, P. J. Ding and W. A. Lanford, *Mater. Res. Soc. Symp. Proc.*, 1994, **337**, 217–224.

35 R. Zahn, M. F. Lagadec, M. Hess and V. Wood, *ACS Appl. Mater. Interfaces*, 2016, **8**, 32637–32642.

36 M. Kim and J. H. Park, *J. Power Sources*, 2012, **212**, 22–27.

37 X. Duan, Y. Han, L. Huang, Y. Li and Y. Chen, *J. Mater. Chem. A*, 2015, **3**, 8015–8021.

38 Q. Pang, D. Kundu, M. Cuisinier and L. F. Nazar, *Nat. Commun.*, 2014, **5**, 1–8.

39 W. Yao, W. Zheng, K. Han and S. Xiao, *J. Mater. Chem. A*, 2020, **8**, 19028–19042.

40 E. H. M. Salhabi, J. Zhao, J. Wang, M. Yang, B. Wang and D. Wang, *Angew. Chem., Int. Ed.*, 2019, **58**, 9078–9082.

41 N. Liu, H. Ma, L. Wang, Y. Zhao, Z. Bakenov and X. Wang, *J. Mater. Sci. Technol.*, 2021, **84**, 124–132.

42 Q. He, B. Yu, H. Wang, M. Rana, X. Liao and Y. Zhao, *Nano Res.*, 2020, **13**, 2299–2307.

43 G. Chen, J. Li, N. Liu, Y. Zhao, J. Tao, G. Kalimuldina, Z. Bakenov and Y. Zhang, *Electrochim. Acta*, 2019, **326**, 134968.

44 H. Ye and J. Y. Lee, *Small Methods*, 2020, **4**, 1900864.

45 C. Li, Z. Li, Q. Li, Z. Zhang, S. Dong and L. Yin, *Electrochim. Acta*, 2016, **215**, 689–698.

46 N. Liu, L. Wang, Y. Zhao, T. Tan and Y. Zhang, *J. Alloys Compd.*, 2018, **769**, 678–685.

47 C. Shen, J. Xie, M. Zhang, P. Andrei, M. Hendrickson, E. J. Plichta and J. P. Zheng, *J. Electrochem. Soc.*, 2019, **166**, A5287–A5294.

48 C. Shen, P. Andrei and J. P. Zheng, *ACS Appl. Energy Mater.*, 2019, **2**, 3860–3868.

49 T. Danner and A. Latz, *Electrochim. Acta*, 2019, **322**, 134719.

50 S. Wang, J. Liao, X. Yang, J. Liang, Q. Sun, J. Liang, F. Zhao, A. Koo, F. Kong, Y. Yao, X. Gao, M. Wu, S. Z. Yang, R. Li and X. Sun, *Nano Energy*, 2019, **57**, 230–240.

51 X. Liang, C. Hart, Q. Pang, A. Garsuch, T. Weiss and L. F. Nazar, *Nat. Commun.*, 2015, **6**, 1–8.

52 X. Huang, Z. Wang, R. Knibbe, B. Luo, S. A. Ahad, D. Sun and L. Wang, *Energy Technol.*, 2019, **7**, 1801001.